Mass transport in turbulent Couette-Taylor flow

W. Y. Tam and Harry L. Swinney
Center for Nonlinear Dynamics and the Department of Physics, The University of Texas, Austin, Texas 78712-9990
(Received 19 March 1987)

We have studied mass transport in a turbulent flow with large coherent structures—turbulent Taylor vortices. A pulse of dye is injected in fluid contained between concentric cylinders (with the inner one rotating and the outer one fixed), and the time dependence of the dye concentration at two axial positions is then determined from optical absorption measurements. The measurements have been made for radius ratios η ranging from 0.494 to 0.875, and at Reynolds numbers R ranging from 50 to 1000 times that corresponding to the onset of Taylor vortex flow. Transport in the axial direction is found to be modeled very well by a one-dimensional diffusion process with the reflections at the ends of the annulus and the finite injection time of the dye taken into account. (The time scale for the transport in the radial and azimuthal directions is short compared with that in the axial direction.) The effective axial diffusion coefficient D in the parameter range studied is of the order of 1 cm^2/s, or greater, orders of magnitude larger than molecular diffusion coefficients. For a fixed R and η, D increases linearly with the axial wavelength λ of the Taylor vortices. The Reynolds-number dependence of the wavelength-independent scaled diffusion coefficient $D^*=(2d/\lambda)D$ (where d is the gap between the cylinders), is described by a power law $D^* \propto R^{\beta}$. Measurements for different parameter regions yield $0.69<\beta<0.86$, while theory suggests a larger value, $\beta=1$.

I. INTRODUCTION

Convective motions result in enhanced transport of mass, heat, etc., on large scales, as in geophysical flows, and on small scales, as in chemical processing.[1] Often the convection leads to transport that is diffusive, but with effective diffusion coefficients that are far larger than the molecular diffusivities. Several recent theoretical papers have considered diffusion in spatially periodic *laminar* flows,[2–4] but less attention has been given to the more difficult problem of transport in *turbulent* flows;[1,5,6] the latter problem is the subject of our work.

We have examined transport at high Reynolds numbers in flow between concentric cylinders with the inner cylinder rotating and the outer cylinder at rest. The Reynolds numbers range from about 100 to 1000 times R_c, where R_c is the Reynolds number corresponding to the primary instability (Taylor vortex flow), and $R=\Omega a d/\nu$; a and Ω are respectively the radius and angular velocity of the inner cylinder, d is the gap between the cylinders, and ν is the kinematic vicosity. At the lower end of the Reynolds-number range the Taylor vortices, although turbulent, are reasonably well defined. However, with increasing Reynolds number the vortex boundaries become increasingly difficult to discern, as the photographs[7] in Fig. 1 illustrate; Smith and Townsend[8] found that the vortices begin to break up for Reynolds numbers above about $700R_c$. Further details on our apparatus and measurements are given in Sec. II, and the analysis of the data is discussed in Sec. IV.

We model the transport in the axial direction as a one-dimensional diffusion process, as discussed in Sec. III. For a one-dimensional random walk with step size L and velocity V, the diffusion coefficient would be given by $D=\frac{1}{2}LV$. We find just such a linear dependence of D on the largest length scale, the vortex wavelength. The dependence of D on the vortex wavelength and Reynolds number is presented in Sec. V, and the results are discussed in Sec. VI.

II. EXPERIMENTAL METHODS

A. Apparatus

A diagram of our Couette-Taylor apparatus is shown in Fig. 2. The outer cylinder, held fixed, was made of precision bore glass. Rotating inner cylinders (made of brass or stainless steel) with four different radii were used, yielding radius ratios η ($\eta=a/b$, where a and b are, respectively, the radii of the inner and outer cylinders) ranging from 0.494 to 0.875. The dimensions for the different cylinders and other parameters are given in Table I.[9]

The inner cylinder was driven through a belt by a stepping motor. The cylinder-rotation rates, measured with a frequency counter, were stable and accurate to better than 0.1% up to the maximum value used, 4500 revolutions per minute. The length of the fluid annulus was fixed by Teflon rings attached to the outer cylinder; the gap between the rings and the inner cylinder was 0.03 cm. Distilled water was used as the working fluid for all the measurements. To control the temperature the entire cylinder system was immersed in a water bath maintained at 20.00 ± 0.05 °C The Joule heating due to rotation of the inner cylinder was negligible, except at very high speeds in the systems with radius ratio 0.730 and 0.875, where it was few tenths of a degree.

Dye was injected through a tube (0.05-cm inner diameter) located at the midheight of the cylinder. The tube was connected to a syringe pump containing methylene blue dye in water. The syringe pump was driven by a

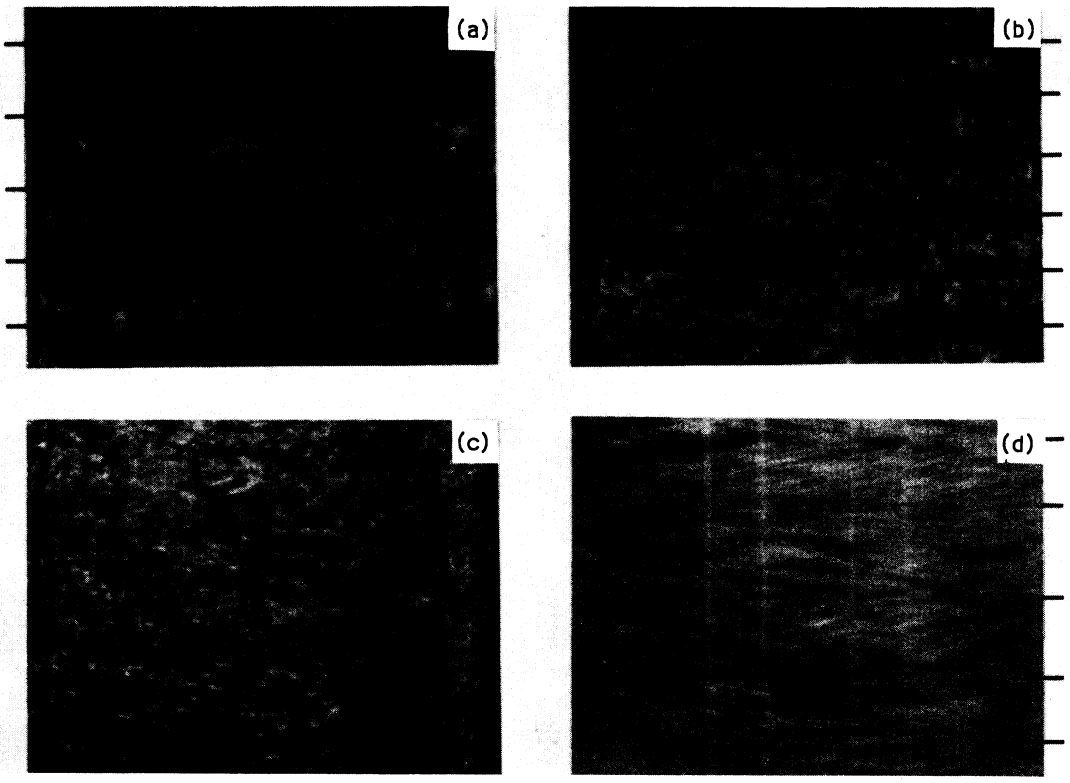

FIG. 1. Photographs of flow between concentric cylinders of radius ratio 0.730: (a) $R/R_c = 50$, (b) $R/R_c = 100$, (c) $R/R_c = 300$ with a short exposure time (0.002 s), and (d) $R/R_c = 300$ with a long exposure time (0.125 s). The boundaries of the Taylor vortices are indicated by the marks at the edges of the photographs. The boundaries are easily discerned in the snapshots at $R/R_c = 50$ and 100, but at $R/R_c = 300$ the boundaries are difficult to discern in a snapshot (c), while they can be seen in a time exposure (d). [The four vertical lines in (d) are reflections from the glass cylinder walls.]

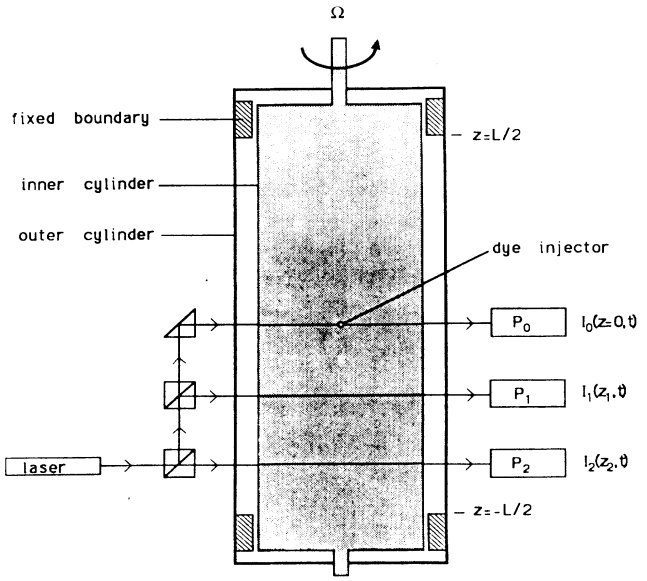

FIG. 2. Schematic diagram of the Couette-Taylor system. $I_0(z=0,t)$, $I_1(z_1,t)$ and $I_2(z_2,t)$ are the transmitted intensities recorded by the photodiodes P_0, P_1, and P_2, respectively.

computer-controlled stepping motor.

The dye concentration was determined as a function of time in optical absorption measurements. The beam from a helium-neon laser was split into three beams which were directed through the gap between the cylinders. One beam, which was at the same level as the injection hole, was used to determine precisely the timing and the profile of the pulse of injected dye. The other two beams, usually 4 cm apart, were located about midway between the injection hole and the lower Teflon ring. The transmitted intensities, measured with three

TABLE I. Parameters for the Couette-Taylor system with length $L = 26$ cm and outer cylinder radius $b = 2.54$ cm: a is the inner cylinder radius, $\eta = a/b$ is the radius ratio, $\Gamma = L/d$ is the aspect ratio (where d is the gap between the cylinders), and the values of R_c are from Ref. 9.

a (cm)	η	Γ	R_c	R/R_c range
1.255	0.494	20	67.3	100–1000
1.603	0.631	28	73.5	50–960
1.854	0.730	38	83.3	75–700
2.222	0.875	82	118.2	50–282

photodiodes, were recorded as a function of time in the computer; the sampling rate varied from 5 to 20 Hz, depending on the rotation rate of the inner cylinder.

B. Procedures

The system was filled with fluid with care to avoid any formation of bubbles. Different ramping procedures were used to produce different numbers of vortices.[10] After equilibrium was reached, the syringe pump was activated to inject a pulse of dye of duration from 0.1 to 1.0 s. Figure 3 shows for a typical run the transmitted intensities recorded by the detectors located at positions z_1 and z_2. Repeated sets of measurements could be made, allowing time for the dye concentration to reach equilibrium between measurements, before the sensitivity decreased significantly due to fluid opacity. At that point a small amount of flow visualization particles (Kalliroscope AQ1000) was introduced into the fluid. After 10 to 30 min it was possible to see the vortices, and the number was counted to obtain the average axial wavelength λ. We could not measure the wavelength of an individual vortex because the boundaries between vortices were not very well defined (see Fig. 1). The whole system was flushed with distilled water several times before starting the next run.

III. MODEL

The transport of dye with concentration $C(\mathbf{r},t)$ in an incompressible flow is governed by

$$\frac{\partial C(\mathbf{r},t)}{\partial t}+\mathbf{v}(\mathbf{r},t)\cdot\nabla C(\mathbf{r},t)=D_{\rm mol}\nabla^2 C(\mathbf{r},t)\ , \tag{1}$$

where $\mathbf{v}(\mathbf{r},t)$ is the fluid velocity and $D_{\rm mol}$ is the molecular diffusion coefficient. If the dye is well mixed in the radial and azimuthal directions on a time scale that is short compared to the time scale for the transport in the axial direction, and if the transport process is studied on length scales large compared to the size of the largest eddies (the vortices), then (1) can be simplified to a one-dimensional diffusion equation,

$$\frac{\partial C(z,t)}{\partial t}=D\frac{\partial^2 C(z,t)}{\partial z^2}\ , \tag{2}$$

where z is the coordinate along the axis of rotation, $C(z,t)$ is the concentration averaged in the radial and azimuthal directions and over an axial distance of the order of a vortex size, and D is the effective axial diffusion coefficient, assumed to be much greater than $D_{\rm mol}$. The assumptions that allow (1) to be written as (2) are examined in Sec. IV and are found to be well satisfied in our work.

For an infinitely long annulus and an injection of δ-function pulse of dye at $(z,t)=(0,0)$, the solution to (2) is

$$C(z,t)=\frac{1}{2\sqrt{\pi Dt}}e^{-z^2/4Dt}\ . \tag{3}$$

For an annulus of finite length, as in the experiments, (3) has to be modified. Our solid Teflon rings at the ends of the annulus impose no-flux boundary conditions at the ends,

$$\left.\frac{\partial C(z,t)}{\partial z}\right|_{z=\pm L/2}=0\ , \tag{4}$$

where L is the length of the cylinder. Furthermore, our measurements show that the profile $u(t)$ of the injected dye (at $z=0$) is well approximated as a rectangular pulse,

$$u(t)=\begin{cases}1, & \text{for } 0<t<\Delta\\ 0, & \text{otherwise}\end{cases}\ , \tag{5}$$

where Δ is the injection duration. With the conditions given by (4) and (5), the solution to (2) is for $t>\Delta$

$$C(z,t)=\frac{1}{2\sqrt{\pi D}}\sum_{n=-\infty}^{\infty}\int_0^{\Delta}\frac{1}{\sqrt{t-t'}}\times\exp\left[\frac{-(z+nL)^2}{4D(t-t')}\right]dt'\ , \tag{6}$$

where $|n|$ is the number of reflections from the ends; the series converges to the accuracy of the measurements with the inclusion of only one or two reflections.

The transmitted light intensity $I(z,t)$ is related to the concentration of the dye by

$$I(z,t)=I_0 e^{-kC(z,t)}\ , \tag{7}$$

where k is a constant proportional to the optical path length of the laser beam passing through the fluid, and I_0 is the transmitted intensity before the injection of dye. Intensity measurements at two positions z_1 and z_2 yield the ratio of concentrations at those positions,

$$\frac{C(z_1,t)}{C(z_2,t)}=\frac{\ln(I_1/I_{01})}{\ln(I_2/I_{02})}\ . \tag{8}$$

Thus we can determine the diffusion coefficient D by fitting the intensity data to (8), where $C(z_1,t)$ and $C(z_2,t)$

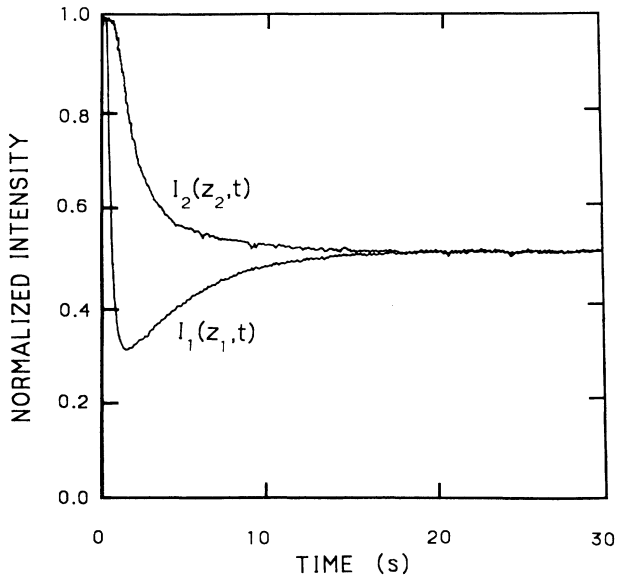

FIG. 3. The time dependence of the normalized transmitted light intensities $I_1(z_1,t)/I_{01}$ and $I_2(z_2,t)/I_{02}$ is shown for a measurement at $R/R_c=282$ (with $\eta=0.875$).

are given by (6). D is the *only* adjustable parameter in this analysis.

IV. DATA ANALYSIS AND SOURCES OF ERROR

The estimated uncertainty in our diffusion coefficient values, determined from averaging the results of many runs, ranges from 5% at the lower Reynolds numbers to 10% at the higher Reynolds numbers. We discuss now the procedure for analyzing the data and the principal sources of error.

A. Data analysis

Time-series measurements of the transmitted intensity were fit to (8) with D adjusted to minimize

$$\sigma^2=\sum_{i=1}^{N}\left[\ln\left[\frac{C(z_1,t_i)}{C(z_2,t_i)}\right]-\ln\left[\frac{\ln[I_1(t_i)/I_{01}]}{\ln[I_2(t_i)/I_{02}]}\right]\right]^2, \tag{9}$$

where N, the number of data points, was 600 or greater. Figure 4 shows examples of these fits for three different Reynolds numbers and radius ratios. For a cylinder system of infinite length and a δ-function injection pulse, these graphs of $\ln[C(z_1,t)/C(z_2,t)]$ *versus* $1/t$ would be straight lines,

$$\ln\left[\frac{C(z_1,t)}{C(z_2,t)}\right]=-\frac{(z_1^2-z_2^2)}{4Dt}, \tag{10}$$

and D could be determined simply from the slope. However, in our system of finite length the reflections from the ends lead to a bend in the curves at small $1/t$, as can be seen in Fig. 4, and the finite duration injection pulse leads to a deviation from a straight line at large $1/t$; the latter effect is fairly small but nonnegligible for our data. The fit of the data to the one-dimensional diffusion model, illustrated by Fig. 4, was found to be excellent throughout the Reynolds-number and radius ratio range studied.

B. Injection effects

The injection of dye perturbs the flow, but measurements with varying amounts of injected dye showed that this small perturbation did not affect the results. The volume of injected dye was typically only 0.01 cm^3, while the volume of a single Taylor vortex was 18 cm^3 for $\eta=0.494$ and 1.5 cm^3 for $\eta=0.875$.

In most of the measurements the dye was injected at a single point. Clearly our assumption of thorough mixing in the azimuthal direction (Sec. III) would be satisfied better if we injected dye at many azimuthal points. To investigate possible limitations of a single injector, two more injectors were added to the outer cylinder at the same axial position as the original injector, but differing in azimuthal position by $+90°$ and $-90°$. Figure 5 shows results for the diffusion coefficient obtained at three Reynolds numbers using one, two, and three injectors. Within the uncertainties of the data there is no dependence on the number of injectors.

C. Injector and probe positions

Another factor to consider is the axial position of the light-intensity probes. For probe positions far from the point of injection, the concentration as a function of z should be described well by the one-dimensional model, (6), even though we have no control of the position of the injector or the probes relative to the vortex boundaries. Near the injector there will of course be significant departures from the model because the time scales for the mixing in the radial and azimuthal directions are comparable to the time scale for the axial transport. On the other hand, the probes should not be too far from the point of injection because with increasing z the sensitivity of the intensity measurements decreases and end effects[11] become significant. Therefore, measurements were made as a function of probe position to determine the optimum position, and results using $\eta=0.730$ are shown in Fig. 6. Diffusion coefficient values independent of z were obtained

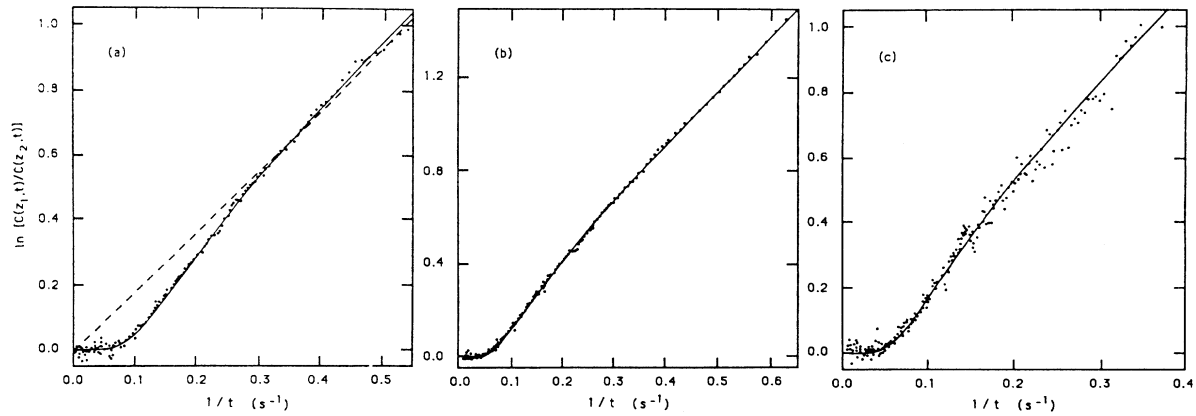

FIG. 4. The time dependence of the ratio of the concentrations at positions z_1 and z_2, determined from measurements of the transmitted light intensity, is compared with the one-dimensional diffusion model [(6)–(8)] for three cases: (a) $R/R_c=500$, $\eta=0.730$; (b) $R/R_c=282, \eta=0.875$; and (c) $R/R_c=800, \eta=0494$. The best fits to the model, shown by the solid curves, yield $D=6.20$ cm^2/s, 4.75 cm^2/s, and 3.94 cm^2/s, respectively, for the three cases. The laboratory system and the model have finite length cylinders and a finite duration injection pulse; in contrast, the behavior for a system with infinitely long cylinders and a δ-function pulse of injected dye would be given by a straight line, as illustrated by the dashed line in (a).

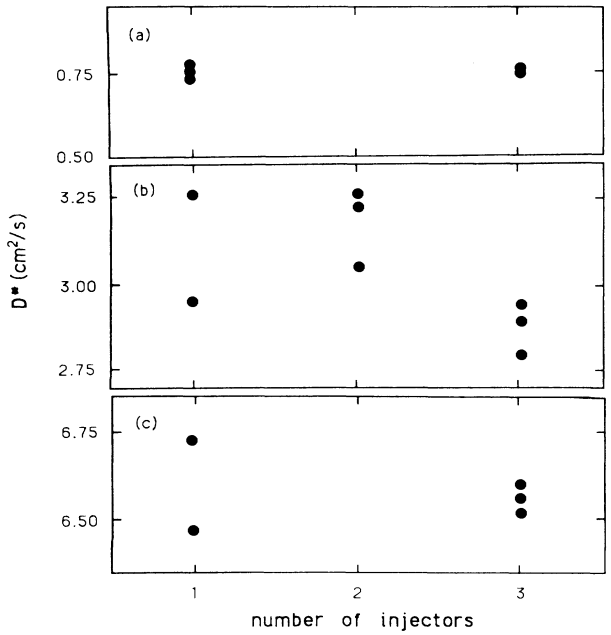

FIG. 5. The effect of varying the number of dye injectors is shown in these results for the scaled diffusion coefficient D^* at (a) $R/R_c=50$, (b) $R/R_c=250$, and (c) $R/R_c=600$, for cylinders with $\eta=0.730$. [D^* is defined in (11).]

with $z_1/d \geq \sim 5$, and good sensitivity was achieved with the probes separated by a distance $\Delta z/d \approx 6$. For smaller values of z_1 the intensity data still fit (6)–(8) fairly well, but the values deduced for the diffusion coefficient become z dependent, decreasing with decreasing z, as Fig. 6 illustrates. Hence, we used the probe positions indicated by the two arrows in Fig. 6 for all other measurements.

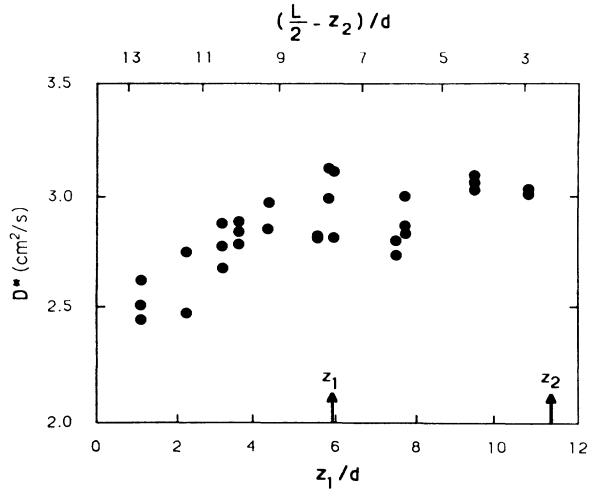

FIG. 6. Measured values of the scaled diffusion coefficient D^*, defined in (11), at $R/R_c=250$ and $\eta=0.730$ are shown as a function of the axial position of the probes: the lower horizontal scale gives the distance of probe P_1 from the injector, and the upper horizontal scale gives the distance of the probe P_2 from the end of the annulus; the separation between the probes was fixed, $\Delta z/d \approx 6$. The arrows indicate the probe locations used in most of our measurements.

We found that the statistical uncertainty in a given measurement of D was always much less than the several-percent scatter between different runs. The latter scatter, evident in Figs. 5–8, arises possibly because of above-mentioned variation in the location of the vortex boundaries relative to the positions of the injector and the probes.

D. Time origin

A source of error at high Reynolds numbers is from the uncertainty in the time of the start of the injection of the dye. At the highest Reynolds numbers, where the intensity decays to the background level in around 10 s, the uncertainty of about 0.1 s in the time origin results in an uncertainty of about 5% in D. In contrast, the values of D were found to be relatively insensitive to the shape of the injection pulse, assumed to be square in our model (5), and to the duration of the injection.

V. RESULTS

The measured values of the axial diffusion coefficients are typically ~ 2 cm^2/s, more than 5 orders of magnitude larger than the molecular diffusion coefficients. Thus the flow produces an enormous enhancement of the transport.

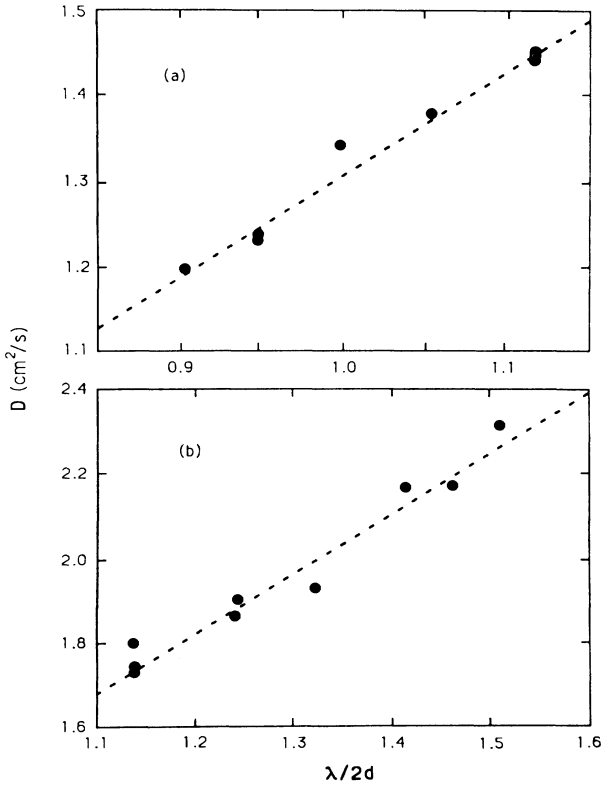

FIG. 7. Results for D as a function of the wavelength λ at (a) $R/R_c=75$, $\eta=0.730$, and (b) $R/R_c=87$, $\eta=0.875$. The dashed lines indicate linear dependence of D on λ.

A. Wavelength dependence

The diffusion coefficient depends on the state of the flow, which is presumably completely specified at the large Reynold numbers of this study by the Reynolds number and the average axial wavelength. At low Reynolds numbers, below those of this study, a complete characterization of a flow would also include the wave numbers for different azimuthal waves.[10,12]

At low Reynolds numbers, stable flows with a range of axial wavelengths were obtained with different ramping procedures that produced different numbers of vortices; e.g., $\lambda/(2d)$ could be varied from 1.1 to 1.5 for $\eta=0.875$. At the highest Reynolds numbers, the number of vortices was apparently unique, although it was difficult then to be certain of the number of vortices because the vortex boundaries were ill defined, as Fig. 1 illustrates.

The measurements as a function of λ at fixed η and R were fit to $D=A\lambda^x$, and it was always found that $x=1$ within the statistical uncertainty; for example, at $\eta=0.875$ and $R/R_c=87$, $x=0.95\pm0.07$. This linear dependence of D on λ is illustrated in Fig. 7 for two cases. Thus with $x=1$, it is convenient to define a scaled diffusion coefficient,

$$D^*=\frac{2d}{\lambda}D\ , \tag{11}$$

which is independent of λ, as illustrated by the data in Fig. 8 for two radius ratios and several Reynolds numbers. All of the data appear to be consistent with (11), although at high R only a narrow range of λ was accessible, and at the highest Reynolds numbers the wavelength dependence could not be determined since stable flows were obtained for only one wavelength value.

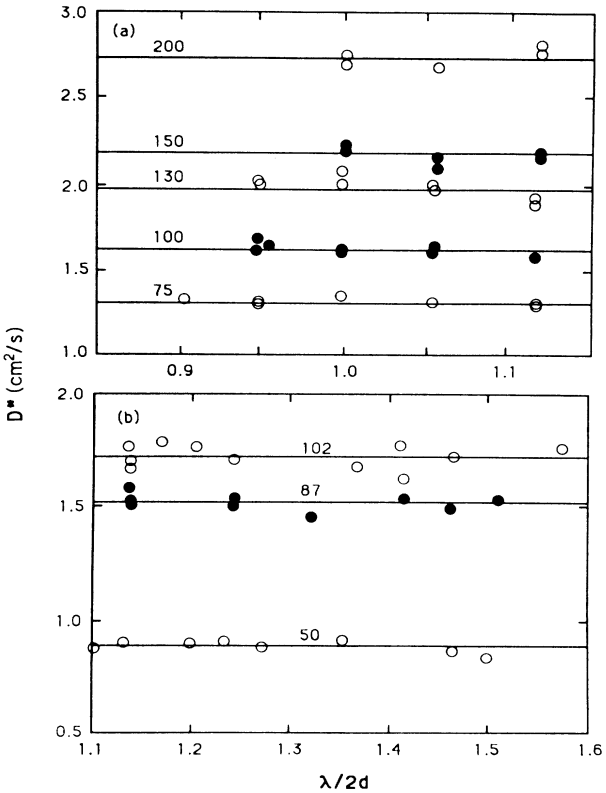

FIG. 8. Results for the scaled diffusion coefficient D^* at different Reynolds numbers, as labeled, for (a) $\eta=0.730$ and (b) $\eta=0.875$. The horizontal lines represent the average values of D^* at different Reynolds numbers.

B. Reynolds number dependence

The values of D^* at each radius ratio increase monotonically with Reynolds number, as shown in Fig. 9, and the behavior is described well by a power law,

$$D^*=D_0^*(R/R_c)^\beta\ . \tag{12}$$

Values of the coefficient D_0^* and the exponent β obtained in nonlinear least-square analyses of the data for different Reynolds number ranges and radius ratios are given in Table II, and the power law is compared with the data for three cases in Fig. 10. The values of D^* also increase monotonically with radius ratio at a given Reynolds number, but this radius ratio dependence has no obvious simple scaling.

Similar values for the exponent β were obtained in fitting the data at radius 0.494, 0.631, and 0.730 over the entire Reynolds number range (R/R_c from about 100 to 1000): 0.69, 0.77, and 0.75, respectively. The data for radius ratio 0.875 extend only to $R/R_c=282$ because of limitations in motor speed. A comparison of values of β obtained in analyses at small R and large R for $\eta=0.631$ and 0.730 suggests that there is a small increase in β with R (see Table II), but the difference is too small to be conclusive, particularly since the uncertainty in the values for D increases with R. In summary, all the data are well described by (12), and the exponent values are in the range $0.69<\beta<0.86$.

VI. DISCUSSION

We know of no previous measurements of diffusion in a spatially periodic turbulent flow. There have been a number of measurements of diffusion in the *radial* direction in flow between concentric cylinders with the inner cylinders

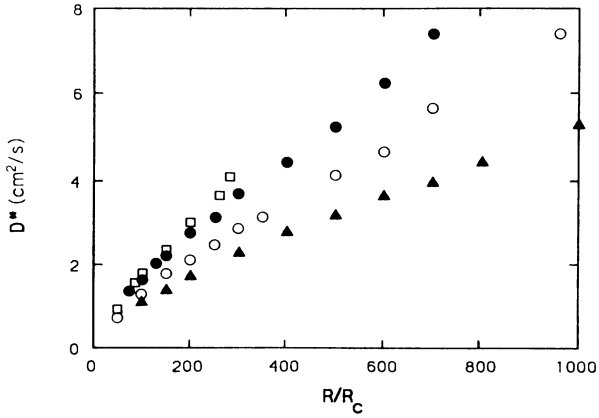

FIG. 9. A plot of D^* (averaged over wavelength) as a function of Reynolds number for $\eta=0.494$ (▲); $\eta=0.631$ (○); $\eta=0.730$ (●); and $\eta=0.875$ (□).

TABLE II. Values of the exponent β obtained in fitting $D^* = D_0^* (R/R_c)^\beta$ to the experimental data for different radius ratios η.

η	R/R_c range	D_0^* (cm^2/s)	β
0.494	all: 100–1000	0.043	0.69
	low: 100–300	0.044	0.69
	high: 300–1000	0.042	0.70
0.631	all: 100–960	0.035	0.77
	low: 100–300	0.047	0.72
	high: 300–960	0.025	0.82
0.730	all: 75–700	0.051	0.75
	low: 75–300	0.057	0.73
	high: 300–700	0.025	0.86
0.875	low: 50–282	0.038	0.85

rotating, but these experiments[13] did not examine transport in the direction of the periodic velocity field, the axial direction (see, however, Ref. 14).

Diffusion in a spatially periodic turbulent flow has been considered theoretically by Zeldovich,[5] who found

$$D = a\lambda V_{\rm rms} , \tag{13}$$

where a is a geometrical factor, λ is the characteristic size of the eddies, and $V_{\rm rms}$ is the rms velocity of the flow. The problem in relating (13) to our experiments is that the dependence of $V_{\rm rms}$ on Reynolds number is not known. It is plausible that the rms velocity is proportional to Reynolds number, but this implies an exponent $\beta = 1$, in contradiction to the experiment.

The result of Zeldovich[5] is formally similar to that obtained by Moffat[1] and Horton[6] for the diffusion coefficient in turbulent flow with no coherent structures,

$$D \sim l_0 u_0 , \tag{14}$$

where l_0 is the first moment of the velocity autocorrelation function and u_0 is the rms fluctuation in the velocity. Again, it is not possible to make contact with experiment since the Reynolds number dependence of l_0 and u_0 are not known.

One way to interpret the observed Reynolds number dependence is as follows. The Kolmogorov microscale[15] κ is proportional to $R^{-3/4}$, while the diffusion coefficient data are described fairly well by $D \propto \lambda R^{3/4}$ (i.e., $\beta = \frac{3}{4}$). This suggests that D is proportional to the ratio of two length scales,

$$D \propto \lambda/\kappa . \tag{15}$$

This scaling should be tested in future experiments, which should include velocity as well as concentration measurements so that the flow-field problem could be separated from the question of the transport of a passive scalar in that flow field. Clearly, more theoretical work as well as experimental work is needed in order to understand the observed Reynolds number dependence.

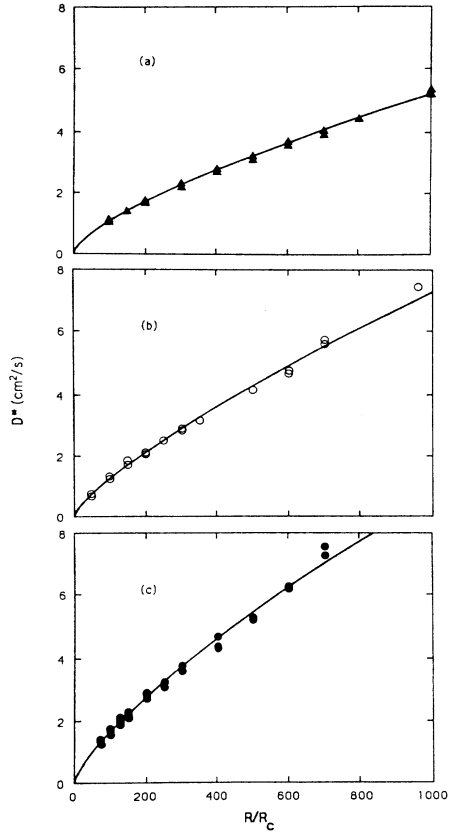

FIG. 10. A comparison of the measured values of the scaled diffusion coefficient with a power law, $D^* = D_0^* (R/R_c)^\beta$, for cylinders with three radius ratios: (a) 0.494, (b) 0.631, and (c) 0.730; the best values of the exponent β for the three cases are 0.69, 0.77, and 0.75, respectively.

In a future experiment it would also be interesting to examine diffusion in turbulent flow between *counter-rotating cylinders* at large Reynolds numbers, where there are no large coherent structures, that is, no Taylor vortices.[16] A comparison of the present results, where the Taylor vortices apparently play a major role in the transport, with measurements for cylinders that are rapidly rotating in opposite directions, where the Taylor vortices are absent, should help elucidate the role of large coherent structures in turbulent diffusion.

ACKNOWLEDGMENTS

We thank Werner Horsthemke and Wendell Horton for numerous helpful suggestions and discussions, and Philip Dixon, Xiang N. Su, and H. Kook for assistance in conducting the experiment. We also enjoyed discussions with Herb Berk, Marshall Rosenbluth, and Boris Shraiman. This research was supported by the U.S. Office of Naval Research Nonlinear Dynamics Program and by the BP Venture Research Unit. W. Y. Tam gratefully acknowledges support by IBM.

[1]H. K. Moffatt, Rep. Prog. Phys. **46**, 621 (1983); J. Fluid Mech. **106**, 27 (1981).
[2]F. Sagues and W. Horsthemke, Phys. Rev. A **34**, 4136 (1986).
[3]B. I. Shraiman, Phys. Rev. A **36**, 261 (1987).
[4]M. N. Rosenbluth, H. L. Berk, I. Doxas, and W. Horton, Phys. Fluids (to be published).
[5]Ya. B. Zeldovich, Sov. Phys.—Dokl. **27**, 797 (1982).
[6]W. Horton, Plasma Phys. Cont. Fusion **27**, 937 (1985).
[7]P. Matisse and M. A. Gorman, Phys. Fluids **27**, 759 (1984).
[8]G. P. Smith and A. A. Townsend, J. Fluid Mech. **123**, 187 (1982).
[9]R. C. DiPrima and H. L. Swinney, in *Hydrodynamic Instabilities and the Transition to Turbulence,* edited by H. L. Swinney and J. P. Gollub (Springer-Verlag, Berlin, 1985), Chap. 6.
[10]M. Gorman and H. L. Swinney, J. Fluid Mech. **117**, 123 (1982).
[11]H. A. Snyder, Int. J. Non-Linear Mech. **5**, 659 (1970).
[12]L. H. Zhang and H. L. Swinney, Phys. Rev. A **31**, 1006 (1985).
[13]D. R. Gabe and F. C. Walsh, J. Appl. Electrochem. **13**, 3 (1983); K. Kataoka, H. Dot, and T. Komai, Int. J. Heat Mass Transfer **20**, 57 (1977); F. Coeuret and J. Legrand, J. Appl. Electrochem. **10**, 785 (1980); J. Electrochim. Acta **5**, 611 (1983); Z. H. Gu and T. Z. Fahidy, J. Appl. Electrochem. **12**, 659 (1982); Chem. Eng. Sci. **40**, 1145 (1985).
[14]Recent measurements of diffusion in Rayleigh-Bénard convection were made for the direction orthogonal to the convection cells, analogous to the axial direction in our experiments. These measurements were made at low Rayleigh numbers where the flow was laminar. See J. P. Gollub and T. H. Solomon, in *Chaos and Related Phenomena: Where Do We Go From Here?,* edited by I. Procaccia (Plenum, New York, 1987).
[15]See, e.g., H. Tennekes and J. H. Lumley, *A First Course in Turbulence* (MIT, Cambridge, Mass., 1972), p. 263.
[16]C. D. Andereck, S. S. Liu, and H. L. Swinney, J. Fluid Mech. **164**, 155 (1986).

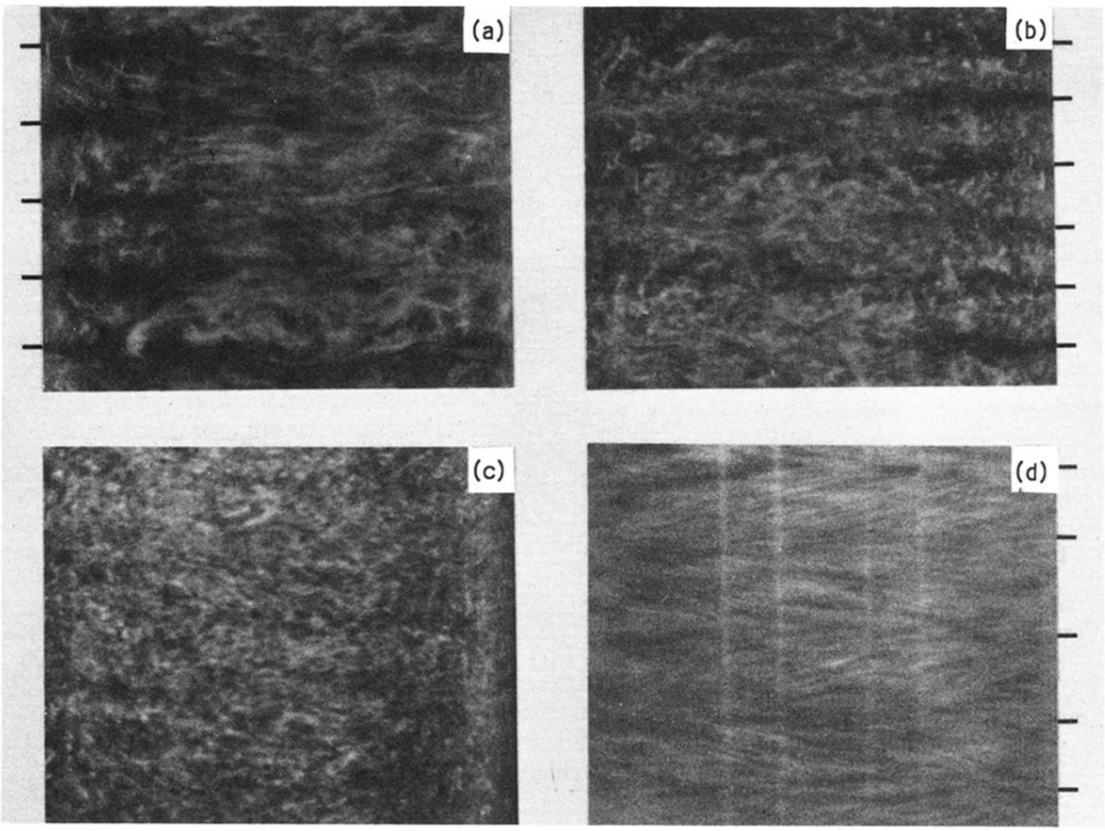

FIG. 1. Photographs of flow between concentric cylinders of radius ratio 0.730: (a) $R/R_c = 50$, (b) $R/R_c = 100$, (c) $R/R_c = 300$ with a short exposure time (0.002 s), and (d) $R/R_c = 300$ with a long exposure time (0.125 s). The boundaries of the Taylor vortices are indicated by the marks at the edges of the photographs. The boundaries are easily discerned in the snapshots at $R/R_c = 50$ and 100, but at $R/R_c = 300$ the boundaries are difficult to discern in a snapshot (c), while they can be seen in a time exposure (d). [The four vertical lines in (d) are reflections from the glass cylinder walls.]

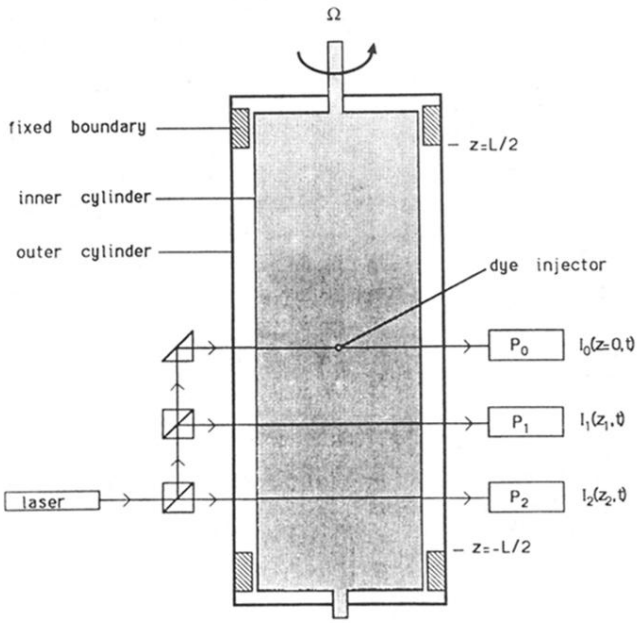

FIG. 2. Schematic diagram of the Couette-Taylor system. $I_0(z=0,t)$, $I_1(z_1,t)$ and $I_2(z_2,t)$ are the transmitted intensities recorded by the photodiodes P_0, P_1, and P_2, respectively.